

Communication

Effects of SiC Content on Wear Resistance of Al-Zn-Mg-Cu Matrix Composites Fabricated via Laser Powder Bed Fusion

Zhigang Shen ¹, Ning Li ^{2,3,*}, Ting Wang ^{2,3} and Zhisheng Wu ¹

¹ School of Materials Science and Engineering, Taiyuan University of Science and Technology, Taiyuan 030024, China

² State Key Laboratory of Advanced Welding and Joining, Harbin Institute of Technology at Weihai, Weihai 264209, China

³ Shandong Provincial Key Laboratory of Special Welding Technology, Harbin Institute of Technology at Weihai, Weihai 264209, China

* Correspondence: 19b909130@stu.hit.edu.cn; Tel./Fax: +86-0631-5687196

Abstract: In this paper, in situ SiC-reinforced Al-Zn-Mg-Cu composites were fabricated by laser powder bed fusion (LPBF). The effects of SiC content on the microstructure, phase composition, microhardness, and wear resistance of as-printed composites were preliminarily investigated. Results show that the microstructure was regulated, the matrix grains were refined, and the tendency to orientation grain growth was suppressed. SiC particles reacted in situ with the Al matrix to produce Si, Al₄C₃, and Al₄SiC₄ phases. The microhardness and wear resistance of as-printed composites increased with SiC content due to the fine grain strengthening of the matrix and the second phase strengthening of precipitates and reinforcements.

Keywords: laser powder bed fusion; aluminum matrix composites; microstructure evolution; microhardness; wear resistance



Citation: Shen, Z.; Li, N.; Wang, T.; Wu, Z. Effects of SiC Content on Wear Resistance of Al-Zn-Mg-Cu Matrix Composites Fabricated via Laser Powder Bed Fusion. *Crystals* **2022**, *12*, 1801. <https://doi.org/10.3390/cryst12121801>

Academic Editors: Hao Yi, Huajun Cao, Menglin Liu and Le Jia

Received: 23 November 2022

Accepted: 8 December 2022

Published: 10 December 2022

Publisher's Note: MDPI stays neutral with regard to jurisdictional claims in published maps and institutional affiliations.



Copyright: © 2022 by the authors. Licensee MDPI, Basel, Switzerland. This article is an open access article distributed under the terms and conditions of the Creative Commons Attribution (CC BY) license (<https://creativecommons.org/licenses/by/4.0/>).

1. Introduction

Aluminum matrix composites (AMCs) have attracted much attention because of their higher specific strength, specific stiffness, and wear resistance compared with aluminum alloys [1,2]. Silicon carbide (SiC) particles are used as reinforcement for AMCs due to their high hardness, wear resistance, and good metallurgical compatibility with aluminum alloy [3,4]. High-strength Al-Zn-Mg-Cu alloy is a pivotal raw material for structural parts, but its high cracking susceptibility during crystallization limits its application [5,6]. SiC-reinforced aluminum matrix composites are the most popular and representative of this system [7]. The mature methods for preparing AMCs include melt stirring, squeeze casting, pressurized infiltration, and vacuum infiltration [8]. However, the mechanical properties of AMCs are often affected by the segregation and settling of SiC particles and weak interfacial bonding between SiC particles and the matrix [9]. Many scholars have proposed improved methods to prepare AMCs with higher performance [10]. Laser powder bed fusion (LPBF) is an innovative strategy for fabricating AMCs due to the advantages of high precision, adjustable raw powder compositions, and direct formability of components [11,12]. Gu et al. [13,14] have prepared AlSi10Mg alloy, AlN/AlSi10Mg composites, and SiC/AlSi10Mg composites by LPBF. Results show that AlSi10Mg alloy has good printability, and the mechanical properties of as-printed composites can be optimized by ceramic reinforcements. However, the low-strength Al-Si alloys could not meet the actual performance requirements. The high-strength Al-Zn-Mg-Cu alloys are a better matrix for the aluminum matrix composites. In this study, SiC-reinforced Al-Zn-Mg-Cu composites were fabricated via LPBF. The effects of SiC content on the microstructure, microhardness, and wear resistance of as-printed composites were investigated. This study made a preliminary attempt to prepare wear-resistant Al-Zn-Mg-Cu composites by LPBF.

2. Materials and Methods

Commercial Al-Zn-Mg-Cu alloy powders ($D_{50} = 38 \mu\text{m}$) with a composition of Al-5.64Zn-2.31Mg-1.40Cu-0.32Fe-0.22Cr-0.08Mn-0.05Si (wt.%) and SiC ceramic powders ($D_{50} = 10 \mu\text{m}$) were used as raw materials. The morphologies and particle size histograms are shown in Figure 1a,b, respectively. The homogeneous composite powders with different SiC fractions (0 wt.%~4 wt.%) were prepared by a planetary shaker-mixer, and the mixing time was two hours. The morphology of 4 wt.% SiC/Al-Zn-Mg-Cu composite powder is shown in Figure 1c. The sphericity of Al-Zn-Mg-Cu alloy powders was not damaged, and SiC particles were uniformly dispersed in Al-Zn-Mg-Cu powders. Table 1 lists the sample labels of the as-printed composites and the corresponding composite powder compositions. Samples for metallographic and performance characterization were printed directly on EOS M290 (Germany, EOS). The schematic of sample orientation is illustrated in Figure 1d. The optimized LPBF parameters for obtaining the high-density as-printed composites are as follows: laser power 340 W, laser scanning speed 800 mm/s, layer thickness 30 μm , and hatch distance 100 μm . The strip-scanning method was adopted with a strip width of 8 mm and a rotation angle of 67°. The schematic of the laser scanning strategy is demonstrated in Figure 1e. Metallographic samples were sanded and mechanically polished layer by layer and then etched with Keller's reagent before being observed. Scanning electron microscopy (SEM, Zeiss) was conducted to scrutinize the microstructure, and the accompanying electron backscattering diffraction (EBSD, EDAX) was employed to analyze the crystallographic features. Samples for EBSD need to be electropolished with a 10% perchloric acid alcohol solution. X-ray diffraction (XRD, DX-2700) was used to analyze the phase composition. Under the loading time of 10 s and loading amount of 100 g, the microhardness of metallographic specimens was measured by Vickers (HV-1000). Wear resistance was investigated on the friction and wear tester (HF-1000), and the schematic is presented in Figure 1f. Before the test, the samples were processed into circular samples with a diameter of 10 mm, polished with 2000 # sandpaper, and cleaned with alcohol. The parameters used are 500 g (load), 560 r/min (rotational speed), and 5 mm (friction diameter). Silicon nitride balls with a diameter of 6 mm and a hardness of 20 GPa were used as the anti-abrasive material. Three groups of tests were conducted to ensure accuracy. The mass before and after testing was measured to obtain the loss of abrasive debris and used to characterize wear resistance.

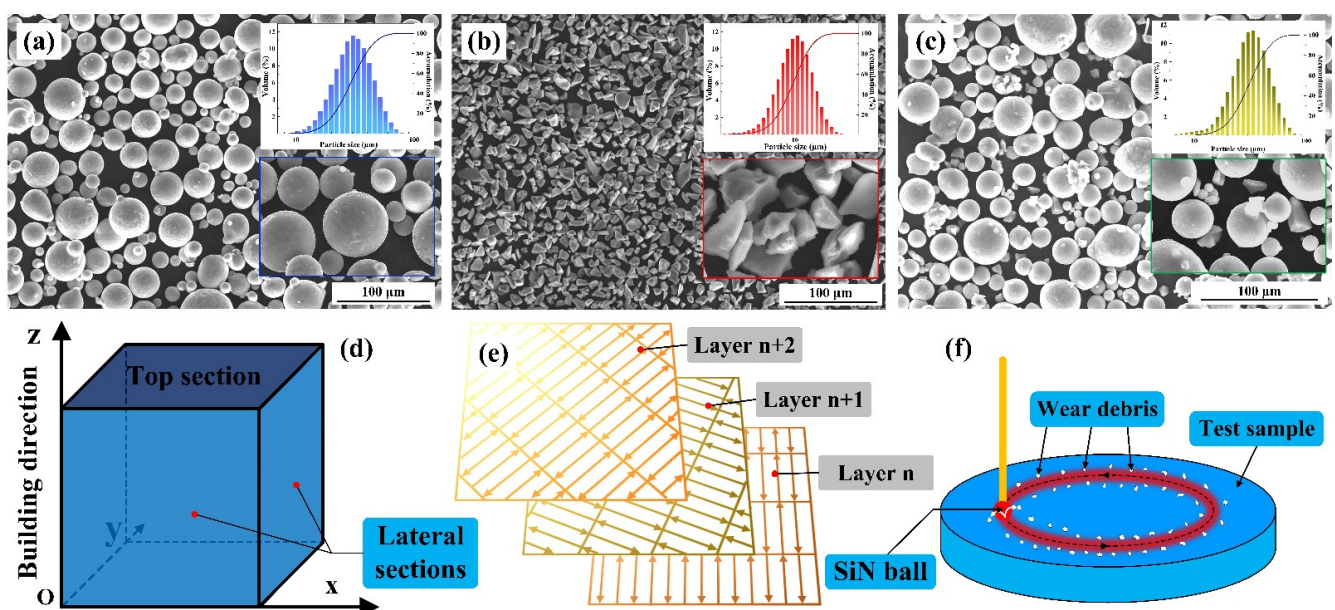


Figure 1. Surface morphologies of (a) Al-Zn-Mg-Cu alloy powders, (b) SiC powders, and (c) 4 wt.% SiC/Al-Zn-Mg-Cu composite powders with insert showing the particle size distribution histogram. Schematics of (d) sample orientation, (e) laser scanning strategy, and (f) friction and wear test.

Table 1. Sample labels of as-printed Al-Zn-Mg-Cu alloy and SiC/Al-Zn-Mg-Cu composites.

Sample Label	Powder Composition
S0	Al-Zn-Mg-Cu alloy
S1	Al-Zn-Mg-Cu alloy + 1 wt.% SiC reinforcement
S2	Al-Zn-Mg-Cu alloy + 2 wt.% SiC reinforcement
S3	Al-Zn-Mg-Cu alloy + 3 wt.% SiC reinforcement
S4	Al-Zn-Mg-Cu alloy + 4 wt.% SiC reinforcement

3. Results and Discussion

3.1. Morphologies and Microstructure

Figure 2 shows the SEM images of as-printed samples with different SiC contents. Fusion lines, cracks, pores, and grain boundaries were scrutinized in the as-printed Al-Zn-Mg-Cu alloy (Figure 2a). These cracks were typical solidification cracks that cracked along the grain boundaries [15]. From the insert (Figure 2b), no precipitates were found at the grain boundaries, and poor intergranular bonding was revealed. Figure 2c presents the microstructure of the S2 sample, where the number of cracks was significantly reduced. A small number of intergranular precipitates were found at the grain boundaries. When the SiC content was 4 wt.%, no cracks were observed within the as-printed composites, as shown in Figure 2d. The irregular SiC reinforcements were uniformly embedded in the matrix without evident agglomeration. Figure 2f shows the XRD diffraction patterns of as-printed samples with different SiC contents. Without SiC reinforcement modification, only the Al phase was detected in the as-printed S0 sample. The as-printed SiC-reinforced Al-Zn-Mg-Cu composites consisted of the Al, SiC, Mg₂Si, Al₄C₃, Al₄SiC₄, and Si phases. During the LPBF process, SiC particles reacted in situ with the Al matrix as follows [16,17].



Al₄C₃, Al₄SiC₄, and Si phases were generated in the molten pool, and some of the generated Si reacted with Mg to form the Mg₂Si phase. Short rod-like Al₄SiC₄ and granular Si-eutectic phases were observed to fill the grain boundaries, as shown in Figure 2e.

Figure 3 illustrates the grain maps, grain size distribution histograms, and pole figures (PFs) of the as-printed S0 and S4 samples, revealing the effects of SiC reinforcement on the matrix grains. The unidentified black regions in Figure 3a,d are cracks and SiC reinforcement, respectively. The coarse columnar crystals (Figure 3a) were refined into fine columnar and equiaxed crystals (Figure 3d) with SiC particles. The size distribution of matrix grains followed unimodal distribution, and the average size was refined from 37.15 μm (S0 sample) to 20.50 μm (S4 sample). Figure 3c,f compare the effect of SiC reinforcement on crystallization textures of the as-printed materials, where A1 is the building direction (BD). The fiber texture of the S0 sample along the [001] crystal orientation parallel to the BD was observed in Figure 3c, predicting the preferential growth of Al grains in the as-printed Al-Zn-Mg-Cu alloy. The maximum value of multiple uniform densities (MUD) was 5.427, which appeared in the (100) crystal plane of the [001] pole figure. The matrix texture was weakened by incorporating SiC particles. For the as-printed S4 sample, the maximum value of MUD was 4.646. For the unmodified Al-Zn-Mg-Cu alloy, the grains were nucleated by attaching to the anterior molten pool and solidified in the building direction. The heterogeneous nucleation effect was noticeable when SiC ceramic particles were introduced.

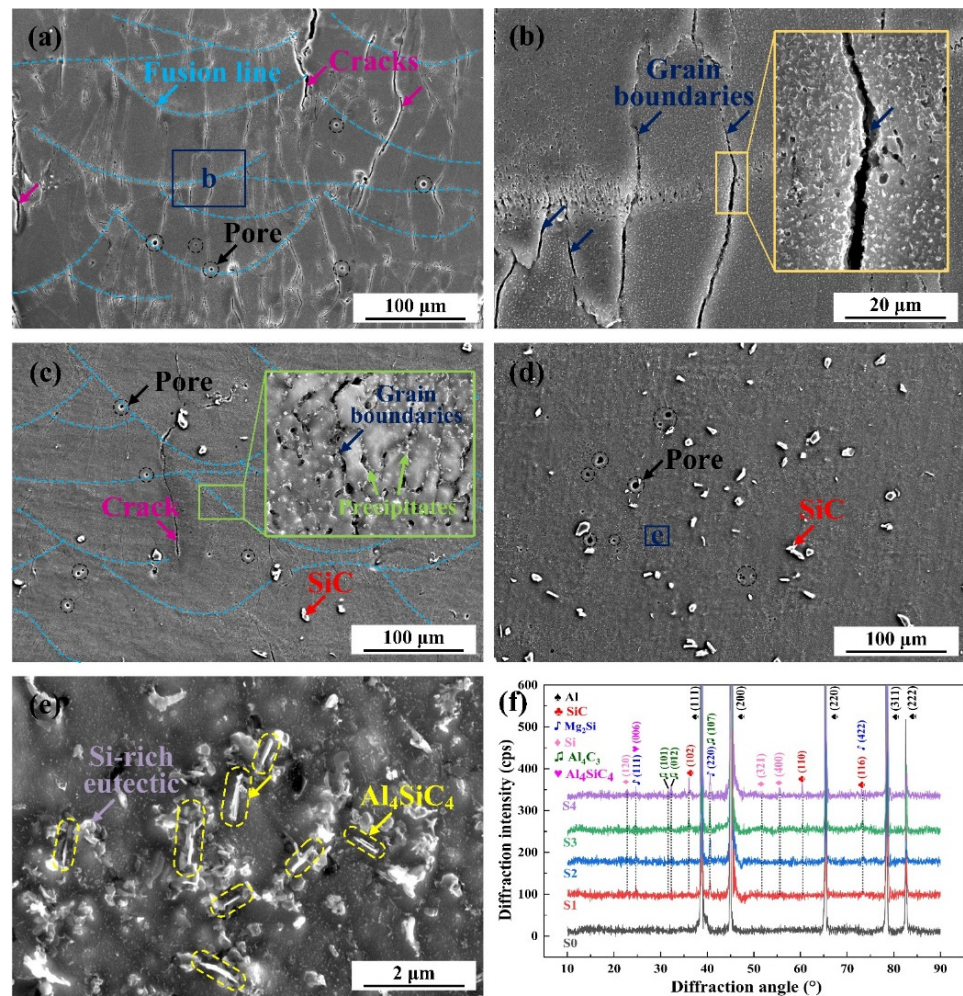


Figure 2. SEM images of the as-printed (a,b) S0 sample, (c) S2 sample, and (d,e) S4 sample. (f) XRD diffraction patterns of the as-printed samples.

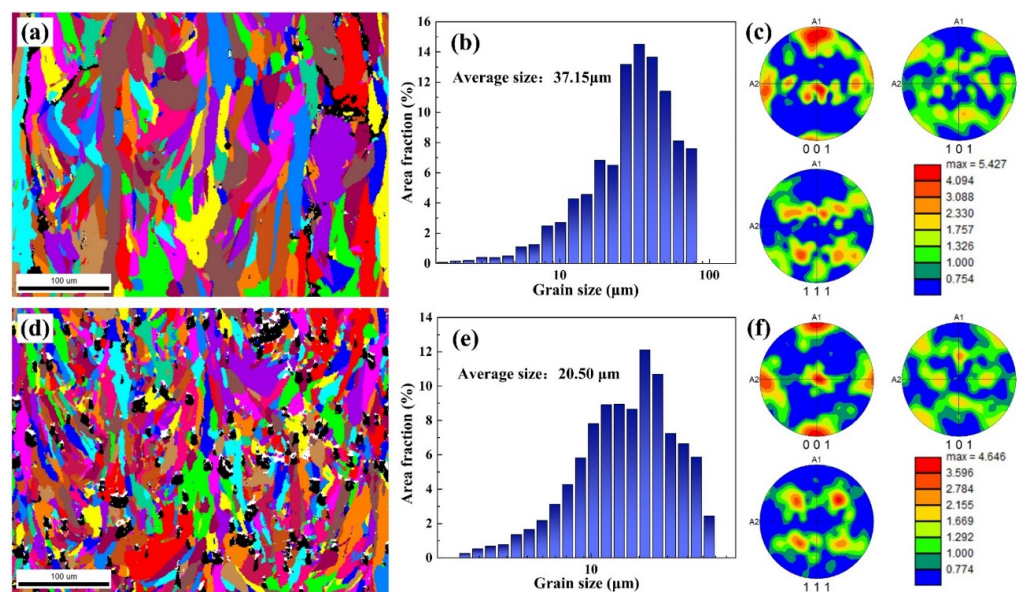


Figure 3. Grain maps, grain size distribution histograms, and PFs along the lateral section of the as-printed (a–c) S0 and (d–f) S4 samples.

3.2. Microhardness

Figure 4 indicates the microhardness of as-printed samples in the lateral and top sections, revealing the effect of SiC particles on the microhardness. The microhardness of the unmodified S0 sample in the side and top sections was 93 ± 5 HV_{0.1} and 102 ± 10 HV_{0.1}, respectively. The microhardness gradually increased with the incorporation of SiC reinforcement. The microhardness of the S4 sample was 156.8 ± 6.4 HV_{0.1} and 161.4 ± 10.5 HV_{0.1}, respectively. Fine grain strengthening of the matrix and particle strengthening of the reinforcement and precipitates were the main reasons for the increased microhardness. The heterogeneity of microhardness was observed along the lateral and top sections, and the top section was higher than the side section. This phenomenon was related to the directional growth of the matrix grains and gradually decreased with increasing SiC content. For the as-printed S0 sample, the lateral section was composed of coarse columnar crystals, and the top section was the fine equiaxed crystal. Fine grain strengthening could be responsible for the difference in microhardness. With the introduction of SiC reinforcement, the columnar grain on the side was gradually refined, and the difference in microhardness was gradually reduced.

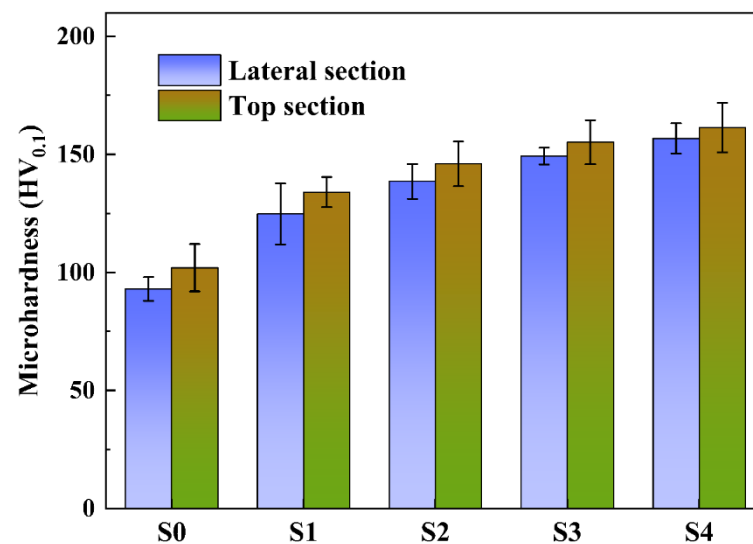


Figure 4. Microhardness histograms of as-printed S0–S4 samples in the lateral and top sections.

3.3. Wear Behavior

The effect of SiC reinforcement on the wear resistance of as-printed AMCs was investigated, and the results are shown in Figure 5. The coefficient of friction (COF) curves are shown in Figure 5a. COF curves showed a similar evolution, characterized by dramatic fluctuations and gradually decreasing with time. Fluctuations might be due to cracks and SiC reinforcement, which could lead to the stripping of the matrix and reinforcement from the sample during friction. The COF curves tended to be stable as the debris with poor binding to the matrix gradually fell off. The average COF values of S0 to S4 samples were 0.507, 0.473, 0.389, 0.348, and 0.288, respectively. The weight loss of the as-printed materials is shown in Figure 5b. The average weight loss for the as-printed S0 to S4 samples were 14.3 ± 1.7 mg, 13.8 ± 1.8 mg, 12.7 ± 2 mg, 9.9 ± 1.2 mg, and 7.6 ± 0.9 mg, respectively. Combining the results of COF and weight loss, the wear resistance of as-printed composites was reinforced with the incorporation of SiC reinforcement. The increase in wear resistance of as-printed composites was mainly due to the synergistic effect of matrix and reinforcement. The hardened SiC ceramic particles could resist the abrasive pressing and improve the deformation resistance of the as-printed composites. The strength of the matrix was increased due to crack inhibition and grain refinement.

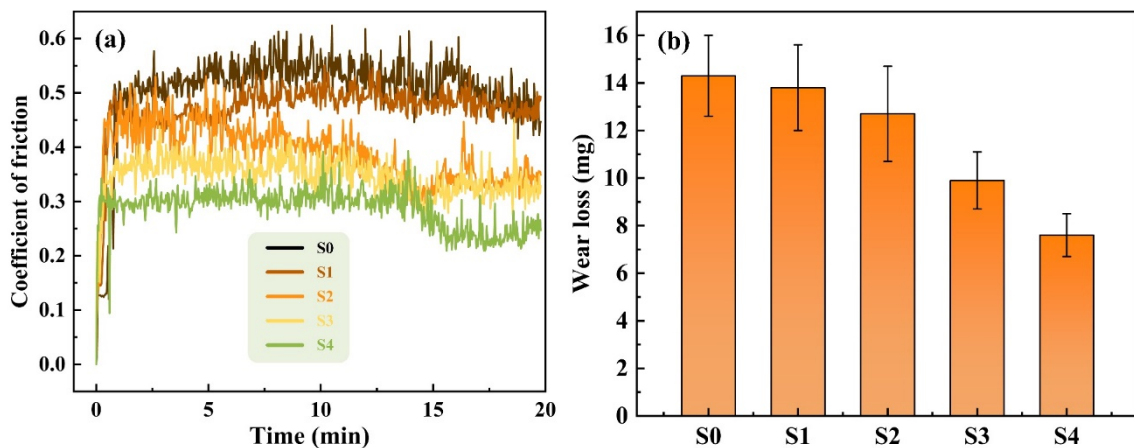


Figure 5. Results of friction and wear. (a) The variation curves of friction coefficient vs. sliding time and (b) the weight loss of the as-printed S0–S4 samples.

4. Conclusions

In this paper, the in situ SiC-reinforced Al-Zn-Mg-Cu composites were prepared by LPBF. The microhardness and wear resistance were reinforced while suppressing the hot cracks. SiC particles reacted in situ with the Al matrix to form Al_4SiC_4 , Al_4C_3 , and Si phases in the molten pool, which precipitated near the grain boundary during solidification. Crack suppression was mainly due to grain refinement, disordered grain growth, and grain boundary structure optimization. The fine grain strengthening of the Al matrix and the second phase strengthening of precipitates and reinforcement were the main reasons for the increase in microhardness and wear resistance.

Author Contributions: Investigation, data curation, Z.S.; investigation, data curation, and writing—original draft preparation, N.L.; supervision, T.W.; equipment management, Z.W. All authors have read and agreed to the published version of the manuscript.

Funding: Please add: This research was funded by the Shandong Provincial Key Research and Development Program, grant number 2019JZZY010439 and the National Natural Science Foundation of China, grant number 52175308.

Data Availability Statement: Not applicable.

Conflicts of Interest: The authors declare no conflict of interest.

References

- Dong, B.-X.; Li, Q.-Y.; Shu, S.-L.; Duan, X.-Z.; Zou, Q.; Han, X.; Yang, H.-Y.; Qiu, F.; Jiang, Q.-C. Investigation on the elevated-temperature tribological behaviors and mechanism of Al-Cu-Mg composites reinforced by in-situ size-tunable TiB_2 -TiC particles. *Tribol. Int.* **2023**, *177*, 107943. [[CrossRef](#)]
- Samal, P.; Vundavilli, P.R.; Meher, A.; Mahapatra, M.M. Recent progress in aluminum metal matrix composites: A review on processing, mechanical and wear properties. *J. Manuf. Process.* **2020**, *59*, 131–152. [[CrossRef](#)]
- Mao, Y.; Li, J.; Vivek, A.; Daehn, G.S. High strength impact welding of 7075 Al to a SiC-reinforced aluminum metal matrix composite. *Mater. Lett.* **2021**, *303*, 130549. [[CrossRef](#)]
- Hu, C.Q.; Du, H.L. Fretting fatigue behaviours of SiC reinforced aluminium alloy matrix composite and its monolithic alloy. *Mater. Sci. Eng. A* **2022**, *847*, 143347. [[CrossRef](#)]
- Klein, T.; Schnall, M.; Gomes, B.; Warczok, P.; Fleischhacker, D.; Morais, P.J. Wire-arc additive manufacturing of a novel high-performance Al-Zn-Mg-Cu alloy: Processing, characterization and feasibility demonstration. *Addit. Manuf.* **2021**, *37*, 101663. [[CrossRef](#)]
- Zhu, Z.; Ng, F.L.; Seet, H.L.; Lu, W.; Liebscher, C.H.; Rao, Z.; Raabe, D.; Nai, S.M.L. Superior mechanical properties of a selective-laser-melted AlZnMgCuScZr alloy enabled by a tunable hierarchical microstructure and dual-nanoprecipitation. *Mater. Today* **2022**, *52*, 90–101. [[CrossRef](#)]
- Ye, T.; Xu, Y.; Ren, J. Effects of SiC particle size on mechanical properties of SiC particle reinforced aluminum metal matrix composite. *Mater. Sci. Eng. A* **2019**, *753*, 146–155. [[CrossRef](#)]

8. Imran, M.; Khan, A.R.A. Characterization of Al-7075 metal matrix composites: A review. *J. Mater. Res. Technol.* **2019**, *8*, 3347–3356. [[CrossRef](#)]
9. Hasan, S.T.; Beynon, J.H.; Faulkner, R.G. Role of segregation and precipitates on interfacial strengthening mechanisms in SiC reinforced aluminium alloy when subjected to thermomechanical processing. *J. Mater. Process. Technol.* **2004**, *153–154*, 758–764. [[CrossRef](#)]
10. Jiang, J.; Wang, Y. Microstructure and mechanical properties of the semisolid slurries and rheoformed component of nano-sized SiC/7075 aluminum matrix composite prepared by ultrasonic-assisted semisolid stirring. *Mater. Sci. Eng. A* **2015**, *639*, 350–358. [[CrossRef](#)]
11. Chen, W.; Xu, L.; Zhang, Y.; Han, Y.; Zhao, L.; Jing, H. Additive manufacturing of high-performance 15-5PH stainless steel matrix composites. *Virtual Phys. Prototyp.* **2022**, *17*, 366–381. [[CrossRef](#)]
12. Koh, H.K.; Moo, J.G.S.; Sing, S.L.; Yeong, W.Y. Use of Fumed Silica Nanostructured Additives in Selective Laser Melting and Fabrication of Steel Matrix Nanocomposites. *Materials* **2022**, *15*, 1869. [[CrossRef](#)] [[PubMed](#)]
13. Dai, D.; Gu, D.; Xia, M.; Ma, C.; Chen, H.; Zhao, T.; Hong, C.; Gasser, A.; Poprawe, R. Melt spreading behavior, microstructure evolution and wear resistance of selective laser melting additive manufactured AlN/AlSi₁₀Mg nanocomposite. *Surf. Coatings Technol.* **2018**, *349*, 279–288. [[CrossRef](#)]
14. Chang, F.; Gu, D.; Dai, D.; Yuan, P. Selective laser melting of in-situ Al₄SiC₄ + SiC hybrid reinforced Al matrix composites: Influence of starting SiC particle size. *Surf. Coatings Technol.* **2015**, *272*, 15–24. [[CrossRef](#)]
15. Li, G.; Li, X.; Guo, C.; Zhou, Y.; Tan, Q.; Qu, W.; Li, X.; Hu, X.; Zhang, M.-X.; Zhu, Q. Investigation into the effect of energy density on densification, surface roughness and loss of alloying elements of 7075 aluminium alloy processed by laser powder bed fusion. *Opt. Laser Technol.* **2022**, *147*, 107621. [[CrossRef](#)]
16. Lu, Q.; Ou, Y.; Zhang, P.; Yan, H. Fatigue performance and material characteristics of SiC/AlSi₁₀Mg composites by selective laser melting. *Mater. Sci. Eng. A* **2022**, *858*, 144163. [[CrossRef](#)]
17. Guo, B.; Chen, B.; Zhang, X.; Cen, X.; Wang, X.; Song, M.; Ni, S.; Yi, J.; Shen, T.; Du, Y. Exploring the size effects of Al₄C₃ on the mechanical properties and thermal behaviors of Al-based composites reinforced by SiC and carbon nanotubes. *Carbon* **2018**, *135*, 224–235. [[CrossRef](#)]